
REAL-TIME LOCALIZATION AND BIMODAL POINT PATTERN ANALYSIS OF PALMS USING UAV IMAGERY

Kangning Cui^{1,2,*}, Wei Tang^{1,2,*}, Rongkun Zhu³, Manqi Wang⁴, Gregory D. Larsen⁴, Victor P. Pauca⁵, Sarra Alqahtani⁵, Fan Yang⁵, David Segurado⁴, Paul Fine⁶, Jordan Karubian⁷, Raymond H. Chan^{2,8,9}, Robert J. Plemmons⁵, Jean-Michel Morel¹, and Miles R. Silman⁴

¹Department of Mathematics, City University of Hong Kong

²Hong Kong Centre for Cerebro-Cardiovascular Health Engineering, Hong Kong

³Department of Computer Science, Xidian University, Xi'an, Shaanxi, China

⁴Department of Biology, Wake Forest University, Winston-Salem, NC, USA

⁵Department of Computer Science, Wake Forest University, Winston-Salem, NC, USA

⁶Department of Integrative Biology, University of California, Berkeley, CA, USA

⁷Department of Ecology and Evolutionary Biology, Tulane University, New Orleans, LA, USA

⁸Department of Operations and Risk Management, Lingnan University, Tuen Mun, Hong Kong

⁹School of Data Science, Lingnan University, Tuen Mun, Hong Kong

ABSTRACT

Understanding the spatial distribution of palms within tropical forests is essential for effective ecological monitoring, conservation strategies, and the sustainable integration of natural forest products into local and global supply chains. However, the analysis of remotely sensed data in these environments faces significant challenges, such as overlapping palm and tree crowns, uneven shading across the canopy surface, and the heterogeneous nature of the forest landscapes, which often affect the performance of palm detection and segmentation algorithms. To overcome these issues, we introduce PalmDSNet, a deep learning framework for real-time detection, segmentation, and counting of canopy palms. Additionally, we employ a bimodal reproduction algorithm that simulates palm spatial propagation to further enhance the understanding of these point patterns using PalmDSNet's results. We used UAV-captured imagery to create orthomosaics from 21 sites across western Ecuadorian tropical forests, covering a gradient from the everwet Chocó forests near Colombia to the drier forests of southwestern Ecuador. Expert annotations were used to create a comprehensive dataset, including 7,356 bounding boxes on image patches and 7,603 palm centers across five orthomosaics, encompassing a total area of 449 hectares. By combining PalmDSNet with the bimodal reproduction algorithm, which optimizes parameters for both local and global spatial variability, we effectively simulate the spatial distribution of palms in diverse and dense tropical environments, validating its utility for advanced applications in trop-

* Kangning Cui and Wei Tang contributed equally to this work. Corresponding author: kangnicui2-c@my.cityu.edu.hk

ical forest monitoring and remote sensing analysis. The dataset can be accessed at [10.5281/zenodo.13822508](https://zenodo.org/record/13822508), and the code to replicate the study is available at github.com/ckn3/palm-ds-sp.

Keywords Environmental Sustainability · Spatial Point Pattern · Object Detection · Instance Segmentation

1 Introduction

Palms (family *Arecaceae*) include many ecologically and economically important species whose spatial distributions crucially inform tropical forest ecology and conservation research. They are also central to local economies and regional to global efforts to incorporate natural forest products into sustainable livelihoods and local to international forest product supply chains [1], [2]. Tropical forests host a significant portion of global biodiversity and are increasingly threatened by deforestation and degradation [3], [4], and palms, with their distinctive ecological importance, can serve as vital indicators of both forest health and human impact, offering insights into biodiversity, soil quality, and the overall health of forest ecosystems [5]. They play a central role in shelter, food, and fiber, and are an emerging resource in the development of non-timber forest product markets, supporting human communities in indigenous and rural areas. Palms also constitute essential and often keystone resources for tropical wildlife [6]–[9]. Here, we are concerned with identifying, locating, and quantifying palms occurring naturally within tropical forests, with particular attention to their spatial distribution and natural reproduction (see Figure 1b), as opposed to palm plantations (see Figure 1a). Knowledge of the spatial distribution and abundance of palms can inform sustainable use and management, leading to economic benefits to local communities. Thus, these tasks are crucial for effective management, economic development, and conservation, as well as for understanding basic ecological questions of palm distribution and abundance.

Palms can be detected in high-resolution remotely sensed imagery by their distinctive leaves and crowns. While object detection and spatial pattern analysis are well-established in computer vision and statistics, applying these techniques to complex real-world environments – such as identifying naturally occurring palms in tropical forests and analyzing their spatial distribution – poses significant challenges [10], [11]. First, palm species are found in highly imbalanced numbers, with certain species being far more prevalent than others [12], [13]. Although various species exist, typically only 2 or 3 species have sufficient number of samples to enable reliable detection. Efficiently detecting all palm species, even the less common ones, is crucial for forest ecology.

Secondly, UAV optical imagery of tropical forests exhibits considerable variability in lighting, occlusion, and background clutter, complicating the analysis process [10], [14]. Palms are often obscured by neighboring tree canopies, making them difficult to detect. Moreover, the dense vegetation in the background and inconsistent lighting across different forest areas further complicates feature detection and localization. Shadows cast by dense canopies and differing sun angles throughout the day lead to significant changes in image brightness and contrast across sampled times and locations, challenging the consistency of algorithmic interpretation [15], [16].

Third, high-quality labeled datasets for realistic environments are notably scarce. The collection and detailed annotation of such data necessitate extensive fieldwork by skilled experts, which is particularly demanding in tropical forests like the Amazon [17]–[19]. The process of annotating and labeling such data typically involves assembling raw imagery into orthomosaics, which are spatially referenced data products derived from UAV captures. However, this process is fraught



Figure 1: Comparative Samples of Manual Labels.

with challenges. Orthomosaics often suffer from noise and artifacts due to image stitching (alignment, merging, and rectification) errors, varying lighting conditions, sensor discrepancies, and environmental factors such as wind and cloud cover, which can lead to movement and shading between images [20].

Moreover, real-time object detection methods for UAV-based remote sensing images are often underutilized, especially in large, densely forested regions where substantial computational resources may be lacking [21], [22]. This shortfall highlights the need for robust, computationally efficient algorithms capable of supporting real-time, on-board UAV processing, which is crucial for numerous field applications.

Finally, large-scale spatial analysis of palms in tropical forests is relatively rare, largely due to limitations in localization methods and the lack of extensive, high-quality datasets. To ensure effective monitoring and conservation, it is crucial to develop robust statistical models that accurately represent the spatial distribution of palms across vast tropical forest areas [5]. Understanding the ecological mechanisms driving plant distribution is fundamental, especially given the urgent need to address the rapid degradation of wilderness areas in recent decades [3], [23].

Addressing the challenges of detecting, segmenting, quantifying, and analyzing the spatial distribution of palms in tropical forests using UAV imagery, this work presents the following main contributions:

1. We develop a dataset through extensive fieldwork across 21 sites in western Ecuador, spanning a rainfall gradient from the Choco’s wettest forests to the edge of the tropical dry forest at the limit of the Sechura desert (5800mm to 1400mm precipitation). This gradient is reflected in the canopy palm species composition and the canopy characteristics of the forests, with dominant species in the northern, wetter sites being absent in the southern, drier sites, and vice versa. We annotate 1,500 image patches from two sites with bounding boxes, capturing 7,356 palm instances, and additionally mark the landscape center points of 7,603 palms across five sites for counting.
2. We introduce a flexible framework for evaluating models in real-time palm detection, segmentation, and counting, effective even with limited computational resources. We further enhance the model’s interpretability using saliency maps to spotlight critical decision-making areas. Additionally, we investigate the balance between label quantity and model performance, revealing that training set size significantly impacts detection but minimally affects counting performance.
3. We present a Poisson-Gaussian reproduction algorithm for simulating the spatial distribution of palms. This model combines a Poisson process with a local Gaussian distribution to accurately replicate observed point patterns. The model provides key insights into ecological dynamics and palm population structures across diverse forest environments.

The paper is organized as follows: Section 2 reviews research on object detection, segment anything models (SAMs), palm identification, and spatial point pattern analysis. Section 3 describes our dataset and methodology, including the study area, data collection, preprocessing, and annotation procedures, and the PalmDSNet framework for palm detection, segmentation, and counting, along with the Poisson-Gaussian model for simulating palm distributions. Section 4 presents our experimental design, numerical results, and analysis of palm localization and spatial distribution. Section 5 summarizes our findings and proposes future research directions.

2 Related Work

2.1 Object Detection

Object detection is a computer vision task aimed at identifying and locating objects within digital images or video frames. This task involves not only classifying the objects but also precisely predicting the location of each object through bounding boxes [24]. Object detection serves as a fundamental step for more complex tasks such as image segmentation, object tracking, and automated scene understanding, underpinning many applications. Two main approaches that have advanced the field are Detection Transformer (DETR) [25], [26] and You Only Look Once (YOLO) [27]–[29].

2.1.1 DETR

Recent developments in object detection have been significantly influenced by the introduction of attention-based transformers, such as DETR [25]. DETR approaches object detection as a set prediction problem, which eliminates the reliance on non-maximum suppression (NMS) and simplifies the detection pipeline. It employs a transformer-based encoder-decoder architecture, combined with a set-based global loss and bipartite matching, to deliver accurate object predictions. The model utilizes a fixed set of learned object queries to capture and reason about the relationships between objects and their global context within the image.

Real-Time Detection Transformer (RT-DETR) [26] enhances the original DETR model by incorporating a convolutional backbone and an efficient hybrid encoder. This adaptation optimizes the processing of multi-scale features through a combination of intra-scale interactions and cross-scale fusion. RT-DETR achieves real-time performance while preserving high accuracy. It also provides flexibility in adjusting inference speed through modifications to decoder layers, without requiring retraining [26].

2.1.2 YOLO

YOLO is a real-time object detection framework that reformulates detection as a single regression task, predicting bounding boxes and class probabilities directly from images. This approach enables rapid processing, making YOLO suitable for applications in various real-world scenarios, such as autonomous driving, robotic navigation, and pedestrian tracking [30]. The YOLO series, particularly versions v8 through v10 [27]–[29], is renowned for its exceptional balance between performance and efficiency.

YOLOv8 [27] introduces a refined architecture that includes a cross-stage partial network for efficient feature extraction, an enhanced path aggregation network for multi-scale feature fusion, and an optimized detection head responsible for predicting object locations and classes in differ-

ent scales [31]. YOLOv9 [28] advances this by incorporating gradient enhanced learning and augmentation network and programmable gradient information to improve training efficiency. YOLOv10 [29] further evolves by eliminating the need for NMS through consistent dual assignments, and features a lightweight classification head, spatial-channel decoupled down-sampling, and a compact inverted block design, which significantly reduces inference latency and makes it the fastest YOLO model to date.

2.2 Segment Anything Model

Segment Anything Models (SAMs) represent a class of advanced segmentation algorithms that can delineate every object within an image, irrespective of its type. Unlike conventional segmentation approaches focused on specific classes, SAMs generalize across varied object types, thus broadening their applicability [32]–[35]. SAMs can segment entire images autonomously or use prompts like points, boxes, or text to direct segmentation. The foundational Segment Anything Model (SAM) [32] and its second generation SAM 2 [33], along with the mobile counterpart Mobile SAM [34], all demonstrate these capabilities.

2.2.1 SAM

The foundational Segment Anything Model (SAM) [32] leverages the SA-1B dataset, which includes over 1 billion masks from 11 million images, to facilitate prompt-based and zero-shot segmentation. SAM integrates a Vision Transformer (ViT) [36] for image encoding, a prompt encoder for processing input prompts, and a dynamic mask decoder for accurate segmentation across various tasks.

The second generation, SAM 2 [33], extends these capabilities to video segmentation, allowing for object tracking across frames. Trained on both the SA-1B dataset and the SA-V dataset, which includes 50.9 thousand videos and 642.6 thousand masklets, SAM 2 enhances performance by incorporating a masked autoencoder (MAE) pre-trained Hiera encoder [37], [38]. This upgrade enables the use of multiscale features, significantly improving the model’s overall effectiveness.

2.2.2 Mobile SAM

Mobile SAM [34] optimizes segmentation for real-time mobile use by employing a simplified image encoder to reduce computational demands. It utilizes a dual-model framework, with a teacher and student model both based on ViT backbones. The encoder’s feature map is processed by a prompt-guided mask decoder to generate segmentation masks. Knowledge distillation [39] trains the student model, minimizing distillation loss: $L_d = \alpha \cdot T^2 \cdot \text{MSE}(\mathbf{p}_t, \mathbf{p}_s) + (1 - \alpha) \cdot \text{MSE}(\mathbf{y}, \mathbf{p}_s)$, where MSE denotes the mean squared error, \mathbf{p}_t are the soft targets from the teacher model at temperature T , \mathbf{p}_s are the outputs from the student model, \mathbf{y} is the ground truth, α balances the losses between soft targets and ground truth, and T adjusts the influence of the soft targets. This approach compresses the SAM model into a more efficient Mobile SAM, enabling its deployment in mobile and resource-constrained environments.

2.3 Palm Identification

Recent advancements in palm identification employ segmentation, classification, and object detection techniques. Segmentation involves dividing an image into polygonal segments that represent different objects or classes; for palm identification, it focuses on isolating palm crowns and iso-

Table 1: Ripley’s G , F , and J Functions. Here, \hat{d}_i represents the nearest neighbor distance for each observed point i , and \tilde{d}_j is the nearest neighbor distance from a simulated point j to the observed points. $\mathbb{1}(\cdot)$ is an indicator function.

Function	Formulation
G	$G(d) = \frac{1}{N_o} \sum_{i=1}^{N_o} \mathbb{1}(\hat{d}_i < d)$, $N_o =$ observed events
F	$F(d) = \frac{1}{N_r} \sum_{j=1}^{N_r} \mathbb{1}(\tilde{d}_j < d)$, $N_r =$ simulated events
J	$J(d) = (1 - G(d))/(1 - F(d))$

lated palm leaves from the background. These methods typically identify the centers of palm features and create a disc-shaped mask around them as ground truth. For instance, Gibril, Shafri, Shanableh, *et al.* utilized a U-Net model with residual networks to segment date palms in UAV images of plantations, characterized by regular palm distributions against bare soil backgrounds [15]. Similarly, Freudenberg, Nölke, Agostini, *et al.* applied two U-Nets of varying complexities to high-resolution satellite imagery of plantations, where palms are regularly spaced and the background is primarily soil [13]. Although the precision and recall in these studies range from 88% to 94%, the scenarios are relatively simple due to the clear backgrounds and regular palm distribution.

Classification techniques assign category labels to entire images, individual pixels, or specific objects within images, such as identifying palm segments based on visual characteristics. A common approach in object detection via classification is the sliding window technique, where a fixed-size window moves across the image to classify each sub-region, though this approach is computationally intensive. Li, Fu, Yu, *et al.* employed CNNs with sliding windows to detect and count oil palms in QuickBird satellite images, benefiting from regular palm distribution and relatively homogeneous, contrasting backgrounds [12]. In Cui, Shao, Larsen, *et al.*, a probabilistic approach was developed to detect palms in high-resolution UAV images of Ecuadorian rainforest, using dual-scale labeling and varying sliding window sizes to create probability maps for palm presence in dense forests [10]. These methods consistently achieve over 95% accuracy in patch classification but require complex postprocessing steps to derive individual palm locations.

Object detection offers a direct approach by using bounding boxes for localization, which demands high-quality annotations, particularly for applications requiring precise and rapid detection. Among the various frameworks available, YOLO is particularly favored for its balance of speed and accuracy [30]. Qin, Wang, Dammer, *et al.* introduced Ag-YOLO, a YOLOv3-Tiny variant with focal loss to improve the detection of smaller areca palms in UAV images [21]. Similarly, Jintasutisak, Edirisinghe, and Elbattay used YOLOv5 to detect date palms in the United Arab Emirates, where palms are clearly delineated against the background [22]. These methods generally achieve precision and recall rates up to 92%, though often tested on smaller datasets with relatively simple backgrounds.

2.4 Spatial Point Pattern Analysis

In forest ecosystems, dynamic ecological processes such as seed dispersal, species competition, and mortality often shape certain spatial patterns for trees that can be detected and modeled [40]. A robust analysis of these spatial distributions is crucial for understanding forest structure and its ecological and evolutionary dynamics [41]–[43]. One natural approach to spatial distribution

analysis involves representing each tree in the study area as a point, and then investigating both (1) the characteristics of the spatial pattern – what the pattern looks like, and (2) the underlying point process that generates the observed data – how the pattern arises.

To address the first question – characterizing point patterns – Ripley’s set of statistical functions, often referred to as Ripley’s alphabet, is widely employed [44], [45]. Among these, three key functions, G , F , and J , stand out for their simplicity and effectiveness. The G function, $G(d)$, calculates the proportion of nearest neighbor distances within the sample that are less than or equal to a given distance d , thereby providing insights into the degree of clustering or dispersion within the data. The F function, in contrast, mirrors the G function but measures the nearest neighbor distances from a set of randomly distributed points to those in the observed pattern, effectively serving as a measure of dispersion between the observed pattern and a completely random one. The J function combines the information from both the G and F functions, offering a more comprehensive analysis by simultaneously considering intra-pattern and inter-pattern spatial relationships. By applying these Ripley’s functions, one can derive clear and concise summary statistics that effectively describe the attributes of point pattern data. Table 1 provides the mathematical definitions of each of these functions.

In addition to functions that consider only the nearest neighbor for each point, there are widely used alternatives designed to detect spatial patterns at multiple scales, such as the K function [44], [46], [47] and its derivative, the L function [48]. These functions, due to their mathematical properties, are highly effective for analyzing multivariate and multi-scale spatial patterns. However, their application is computationally intensive and requires comprehensive data collection across large areas [49], [50]. Since our research is focused on a specific and confined region of palm distribution, we prioritize single-scale functions to optimize efficiency while still capturing relevant spatial patterns.

In simulating the process that generates the observed spatial patterns, it is advantageous to employ mathematical point process models that incorporate stochastic mechanisms. The homogeneous Poisson process, widely used in ecological studies [51], [52], assumes that points are randomly and independently distributed within the observation window, leading to point patterns that exhibit complete spatial randomness with no spatial trends or associations among points. However, this simplistic model often fails to capture the complexity of real-world environmental conditions. To address this limitation, more advanced models have been developed. In contrast to the homogeneous Poisson process which assumes a constant intensity, the heterogeneous Poisson process employs a spatially varying intensity function, enabling a closer approximation of real-world data distributions [52]–[54]. Additionally, the Thomas cluster process, a widely adopted model, introduces Poisson cluster processes across multiple scales, thereby enhancing the model’s capacity to depict the intricate structures observed in empirical data [55], [56].

3 Materials and Methods

3.1 Dataset

3.1.1 Study Sites and Data Collection

The data for this study come from tropical forest in western Ecuador Chocó centered on the Fundación para la Conservación de los Andes Tropicales Reserve and adjacent Reserva Ecológica Mache-Chindul park (FCAT; 00°23’28” N, 79°41’05” W), and the Jama-Coaque Ecological Re-

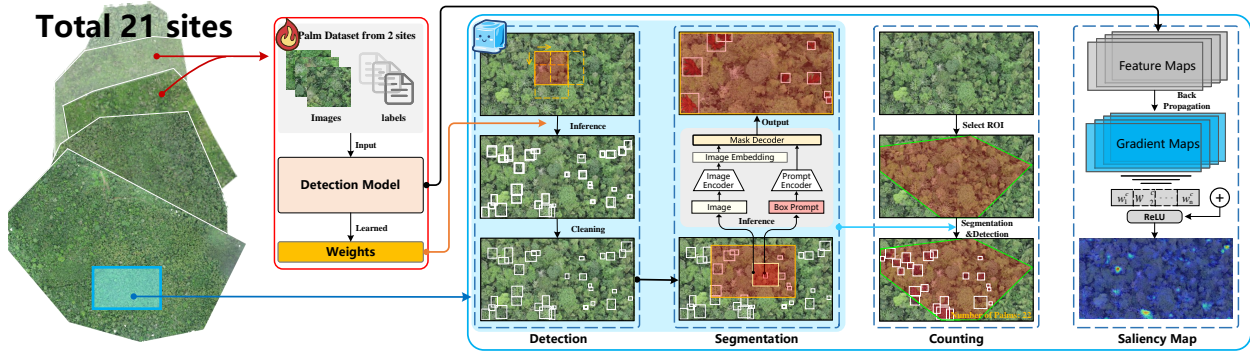


Figure 2: Workflow of PalmDSNet. The model is trained on labeled patches for accurate palm detection, with the refined weights then used to infer bounding boxes on new images. These boxes guide the segmentation and counting processes across selected regions or landscape scales. Saliency maps are also produced to enhance the interpretability of palm localization.

serve (00°06'57" S, 80°07'29" W). The FCAT reserve is high diversity humid tropical forest at ~ 500 m elevation, receiving ~ 3000 mm precipitation yr^{-1} accompanied by persistent fog during the period of lower precipitation. The Jama-Coaque reserve spans from the boundary of tropical moist deciduous/tropical moist evergreen forest at the lower elevations (~ 1000 mm precipitation yr^{-1} , ~ 250 m asl) to fog-inundated wet evergreen forests above 580m to 800m. These forests harbor several regularly occurring palm species with canopy-exposed crowns [57], [58], with the dominant species being *Iriartea deltoidea* and *Socratea exorrhiza* at FCAT and *Astrocaryum standleyanum* and *Socratea exorrhiza* at Jama-Coaque.

To capture detailed spatial data, UAV operations were conducted in two phases across 96 plots in 21 areas, covering a total of 1995 hectares with a ground spacing distance (GSD) < 6 cm. The first phase, in June 2022, involved flying over 95 hectares using a DJI Phantom 4 RTK drone equipped with a 1" CMOS sensor. Mission planning was done using GS RTK, with flights conducted at an altitude of 90 meters above ground level (AGL) with 70% sidelap and 80% frontlap, resulting in 387 photos processed with Agisoft Metashape 2.0 to produce orthomosaics. An orthomosaic is a large, georeferenced image created through photogrammetry, compiled from multiple overlapping images of a specific geographic area. These images are orthorectified to standardize perspective and spatial scale while embedding spatial metadata. However, localized distortions may occur, particularly along the edges due to the orthorectification process. The second phase, conducted in February 2023, expanded coverage to 1900 hectares, flying at 150 meters AGL and capturing 8458 photos using the same drone and software. Subsequent data processing involved noise reduction, edge trimming of orthomosaics, and the generation of Digital Surface Models and Digital Terrain Models.

3.1.2 Manual Labels

To develop a high-quality training and validation dataset for our models, we manually labeled drone imagery from two sites within the FCAT Reserve. We extracted 800×800 patches from orthomosaics, selecting a subset of 1,500 patches representing various image qualities and palm densities. Precise bounding boxes were annotated around palm crowns and isolated leaves. Additionally, for counting purposes, we manually labeled five orthomosaics using ArcGIS Pro 3.3.1, systematically placing georeferenced points at the centers of palm crowns visible in the canopy imagery.

Unlike studies focused on regularly spaced plantation palms [12], [15], [22], our research examines natural forest data (see Figure 1). The manual annotation of bounding boxes was particularly hard due to palms overlapping with one another and other trees, and the occurrence of artifacts and distortion from orthomosaic processing. Similarly, labeling the center points of palms across five sites was labor-intensive but essential for conducting landscape-level analysis and validating our model’s counting accuracy against expert assessments.

3.2 Palm Detection and Segmentation Network

This section introduces the Palm Detection and Segmentation Network (PalmDSNet), a framework specifically designed to detect, segment, and count palms in the dense and diverse tropical forests (see Figure 2). Unlike previous approaches that either convert detection into segmentation [13], [15], treat it as a classification task [10], [12], or focus solely on detection without segmentation [21], [22], our approach employs a state-of-the-art detection model enhanced with an integrated segmentation head. Additionally, our framework tackles the complexities of dense rainforests with irregular palm distribution and overlapping vegetation, demonstrating the ability to locate palms even from a single leaf, by applying it to a dataset containing these challenging images.

PalmDSNet is a flexible architecture that allows for substitution of different detection and segmentation methods to suit various contexts. We employ fine-tuned backbones for palm detection, followed by segmentation models to delineate the detected palms, visualizing their spatial distribution. The detection results are refined for precise counting, which is displayed alongside segmentation maps to provide a comprehensive overview. Moreover, we enhance result interpretability using saliency maps, which highlight the focal areas influencing the detection network’s decisions. This multi-phase approach combines state-of-the-art object detection and segmentation models to achieve accurate, real-time palm counting.

3.2.1 Palm Detection

We train networks to locate palms within forest landscapes depicted in orthomosaic images, which are segmented into patches for detailed analysis. These networks are designed to be flexible, allowing for the substitution of alternative models, such as YOLOs or DETRs [25]–[29], based on specific analytical needs. Training involves various image augmentations, such as adjustments in hue, saturation, and brightness, as well as rotations, scaling, translations, and flips, to enhance model robustness across diverse environments. During inference, each patch is analyzed to locate palms, with their coordinates recorded for further processing. NMS is employed to eliminate redundant detections from overlapping patches, ensuring that each identified palm is uniquely processed in the subsequent segmentation phase.

3.2.2 Palm Segmentation

Segmentation is performed during inference due to the absence of segmentation masks in the training dataset. Detected palms serve as centers, with their surrounding areas included for contextual information. The bounding box from the detection phase acts as a prompt for a chosen SAM, guiding it to accurately segment the palm. This method is particularly efficient for focusing on specific regions within extensive forest landscapes.

3.2.3 Palm Counting

Palm counting starts by defining the scope of analysis, which can be the entire landscape or a specific region of interest (ROI). For ROIs, a user-drawn polygon is enclosed within a rectangular bounding box to ensure full coverage during detection and segmentation. The detection module identifies individual palms and logs their coordinates, followed by redundancy removal using NMS. The segmentation branch then generates masks for these palms based on detection outputs. These masks, along with the bounding boxes, are visualized to enable thorough analysis and verification of detected palms within the ROI.

3.2.4 Saliency Map

To enhance model interpretability and reliability, we use Grad-CAM [59], [60]. This technique creates a coarse localization map by leveraging gradients flowing into the final convolutional layer, highlighting the regions of the image most crucial for predicting the target concept. Grad-CAM provides visual explanations for the model’s predictions, revealing key areas of focus and ensuring that the network emphasizes relevant features for accurate palm localization.

3.3 Poisson-Gaussian Palm Reproduction Algorithm

This section introduces the proposed Poisson-Gaussian model to simulate palm spatial reproduction that optimizes the reproduction parameters to minimize the discrepancy between observed and simulated point patterns of palm coordinates (see Algorithm 1). By utilizing this model, we aim to gain insights into both global and local aspects of palm reproduction, including long-range and short-range reproductive dynamics. Understanding the spatial distribution of palms within tropical forests can further reveal the relationships among different palm species and individuals of the same species, ultimately helping to determine whether palms compete for resources or can coexist in close proximity.

The proposed Poisson-Gaussian model integrates a Poisson point process [61] with a local Gaussian distribution to simulate the dual nature of palm propagation. The Poisson point process captures the random spread of palms, such as through animal-mediated dispersal or other stochastic processes, leading to a more uniform distribution of individuals. The Gaussian distribution, on the other hand, represents the tendency of seeds to fall and germinate near their parent trees, reflecting a more localized clustering effect. By adjusting these processes to align with observed spatial patterns, the model provides insights into the ecological dynamics and spatial organization of palm populations in tropical forests. This proposed approach is preferable to the Student’s t distribution [62], as it generates fewer local samples while allowing a portion of samples to disperse globally, thus better aligning with the concept of negative density dependence (NDD) [63]. NDD posits that as population density increases, the probability of seed germination and survival decreases, encouraging species coexistence and spatial distribution patterns more reflective of ecological realities.

The optimization process begins with initializing p^* and σ^* to zero and setting d_{min} to infinity. Ripley’s function g and the empirical distribution function f are computed for the observed set X , serving as benchmarks for comparison. The `Simulate` function then generates synthetic point patterns based on candidate values of p and σ . The simulation starts with a single randomly placed point and probabilistically adds new points: with probability p , offspring are drawn from a Gaussian distribution centered around a randomly selected parent, and with probability $1 - p$, offspring are uniformly distributed. This process continues until the synthetic set \hat{X} matches the size of X .

Algorithm 1: Poisson-Gaussian Palm Reproduction

Input: \mathbf{p} (list of candidate p), $\boldsymbol{\sigma}$ (list of candidate σ), X (set of observed palm coordinates), N (number of Simulations)

Output: p^* , σ^* (optimal p and σ that minimizes d)

```
1 Initialize  $p^* = 0, \sigma^* = 0, d_{min} = \infty, \hat{X} = \emptyset$ ;  
2 Compute Ripley's functions  $\mathbf{g} = G(X)$  and  $\mathbf{f} = F(X)$ ;  
3 Procedure Simulate( $p, \sigma$ ):  
4   Initialize  $\hat{X}$  with a random 2D point generated uniformly across the spatial extent;  
5   while  $|\hat{X}| < |X|$  do  
6     Select a random parent palm  $\mathbf{x}$  from  $\hat{X}$  and generate a random number  $p_r$  from  $[0, 1]$ ;  
7     if  $p_r < p$  then  
8       Generate offspring palm using a Gaussian distribution  $\mathcal{N}(\mathbf{x}, \boldsymbol{\Sigma})$  around the parent  
9        $\mathbf{x}$  with  $\boldsymbol{\Sigma} = [\sigma^2, 0; 0, \sigma^2]$ ;  
10    else  
11     Generate offspring palm from a 2D uniform distribution;  
12    end  
13    Append offspring palm to  $\hat{X}$ ;  
14  end  
15  return  $\hat{X}$ ;  
16 foreach  $p$  in  $\mathbf{p}$  do  
17   foreach  $\sigma$  in  $\boldsymbol{\sigma}$  do  
18     Initialize  $d = 0$ ;  
19     for  $i = 1$  to  $N$  do  
20        $\hat{X}_i = \text{Simulate}(p, \sigma)$ ;  
21       Compute  $\mathbf{g}_{s_i} = G(\hat{X}_i)$  and  $\mathbf{f}_{s_i} = F(\hat{X}_i)$ ;  
22       Integrate the difference for the  $i$ -th trial:  $d_i = \int_x |\mathbf{g} - \mathbf{g}_{s_i}| dx + \int_x |\mathbf{f} - \mathbf{f}_{s_i}| dx$ ;  
23        $d = d + d_i$ ;  
24     end  
25     if  $d < d_{min}$  then  
26       Update  $d_{min} = d, p^* = p, \sigma^* = \sigma$ ;  
27     end  
28 end  
29 return  $p^*, \sigma^*$ ;
```

For each parameter combination, N simulations are performed to compute the total discrepancy. Simulated patterns are compared to the observed data using Ripley's function and the empirical distribution function. The discrepancy d_i for each trial is measured as the integral of absolute differences between observed and simulated functions. The total discrepancy d is the aggregate of discrepancies across all trials, with the optimal parameters identified as those minimizing d . This optimization framework effectively balances local clustering with global dispersion patterns to best replicate the observed spatial distribution of palms.

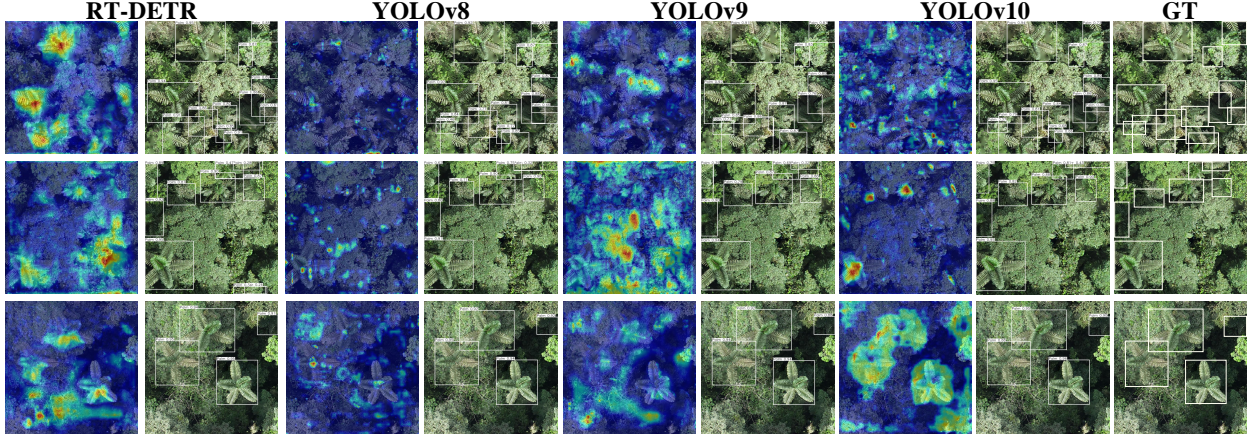


Figure 3: Comparative Visualization of Detection Outcomes and Saliency Maps Across Different Models in PalmDSNet. Each pair of columns displays detection results with bounding boxes and confidence levels alongside saliency maps derived from detection model weights. The final column showcases the labeled ground truth (GT).

4 Experimental Results

This section outlines the performance evaluation of our PalmDSNet framework, systematically addressing several research objectives across different ecological sites. Initially, we investigate the performance of various detection models, including RT-DETR [26], YOLOv8 [27], YOLOv9 [28], and YOLOv10 [29] under diverse training conditions to understand their accuracy and efficiency. Saliency maps [59] are utilized to help understand the focus regions of different models for palm detection in densely populated tree crowns. Following detection, we assess the capabilities of segmentation models SAM [32], SAM 2 [33], and Mobile SAM [34], focusing on their inference time and the visual quality of segmentation results. We then explore the impact of training data volume on the accuracy of these models and evaluate their counting performance, a critical component for ecological analysis. Finally, we apply these models to orthomosaics to assess their efficiency in real-time, large-scale landscape analysis.

Additionally, we evaluate our proposed bimodal palm reproduction model, which combines a Poisson point process with a local Gaussian distribution. This model simulates the spatial distribution of palms by accounting for both random spread and localized clustering effects. By comparing simulated patterns with observed data, we assess how well the model replicates real-world palm distribution. This evaluation provides valuable insights into the ecological dynamics of palm populations, including interspecies interactions and habitat coexistence, enhancing our understanding of palm community structuring in tropical forests.

Table 2: Performance Comparison of Detection Models for PalmDSNet.

Model	GFLOPS	Params (M)	Latency (ms)	Validation (10% Training)					Validation (90% Training)				
				Precision	Recall	AP ₅₀	AP ₇₅	mAP	Precision	Recall	AP ₅₀	AP ₇₅	mAP
RT-DETR	222.5	65.5	22.4	0.845	0.778	0.843	0.560	0.532	0.923	0.905	0.955	0.822	0.734
YOLOv8	257.4	68.1	22.9	0.859	0.773	0.849	0.569	0.532	0.902	0.919	0.944	0.725	0.672
YOLOv9	189.1	57.4	24.3	0.869	0.795	0.878	0.640	0.590	0.897	0.914	0.950	0.769	0.680
YOLOv10	169.8	31.6	21.2	0.838	0.781	0.846	0.562	0.529	0.912	0.891	0.938	0.735	0.662

Table 3: Effectiveness of Different Configurations for PalmDSNet Across 5 Sites. Sites marked with * are training locations.

Site	Size (ha)	No. of Counts	Counting Accuracy (10% Training)				Counting Accuracy (90% Training)			
			RT-DETR	YOLOv8	YOLOv9	YOLOv10	RT-DETR	YOLOv8	YOLOv9	YOLOv10
FCAT 1*	21.7	284	0.997	0.979	0.997	0.993	0.989	0.997	0.997	0.993
FCAT 2*	119.4	2,569	0.998	0.988	0.992	0.994	0.999	0.998	0.998	0.997
FCAT 3	103.1	2,206	0.998	0.995	0.993	0.995	0.999	0.998	0.998	0.995
Jama-Coaque 1	112.2	732	0.969	0.876	0.872	0.862	0.975	0.870	0.909	0.833
Jama-Coaque 2	92.3	1,596	0.938	0.776	0.812	0.775	0.940	0.743	0.824	0.791

4.1 Experimental Setting

To assess the performance of both PalmDSNet and our bimodal reproduction model, we conducted a series of experiments to ensure robustness and reliability. For PalmDSNet, two distinct data allocation strategies were tested: one using 10% of the data for training over 100 epochs to evaluate performance with limited samples, and another using 90% of the data for training over 300 epochs to maximize data utilization. Both trained models were then used to validate the detection and counting performance. Images were cropped to 800×800 pixels, providing a broader receptive field, with a stride of 400 for efficient inference on large orthomosaic images. The model was configured to detect a single class to simplify the architecture and reduce computational requirements. While four RTX 3090 GPUs were utilized for training, only one was used during validation and testing to simulate the constraints of real-time operational settings.

For the Poisson-Gaussian palm reproduction model, we conducted simulations on a CPU, specifically an Intel Xeon Silver 4210 with 40 cores running at 2.20 GHz, to evaluate its ability to replicate the spatial distribution of palms. Each simulation was performed 10 times ($N = 10$) to ensure that the results were not influenced by random variation. The Ripley’s functions, which quantify spatial patterns, were computed at sampled x-axis coordinates. The trapezoidal rule [64] was then employed to interpolate these functions and integrate the absolute differences between observed and simulated distributions.

Our evaluation utilized a series of standard metrics for a thorough assessment of the model’s performance. Precision and Recall measure the model’s accuracy and error rates in detecting objects. Average Precision (AP) at various IoU thresholds quantifies precision across different recall levels, and Mean Average Precision (mAP) aggregates these measures for a comprehensive performance overview. We also examine computational demands by comparing Giga Floating Point Operations Per Second (GFLOPS), the number of parameters (Params), and latency to evaluate efficiency during training and real-time inference. We validate the model’s counting ability by comparing its performance on five sites against that of human experts. For the bimodal reproduction model, we used the minimum integrated difference between observed and simulated point patterns to determine the optimal parameter pair p^* and σ^* .

4.2 Performance Evaluation of PalmDSNet

4.2.1 Detection

The comparative analysis of detection models for PalmDSNet are encapsulated in Table 2, highlighting model size, inference latency, and performance metrics under two distinct training scenarios: 10% and 90% of the data used for training. The evaluated models demonstrate diverse computational costs and inference efficiencies. YOLOv10 emerges as the lightest with the fewest parameters and lowest GFLOPS, whereas YOLOv8 is the heaviest. Despite the differences in

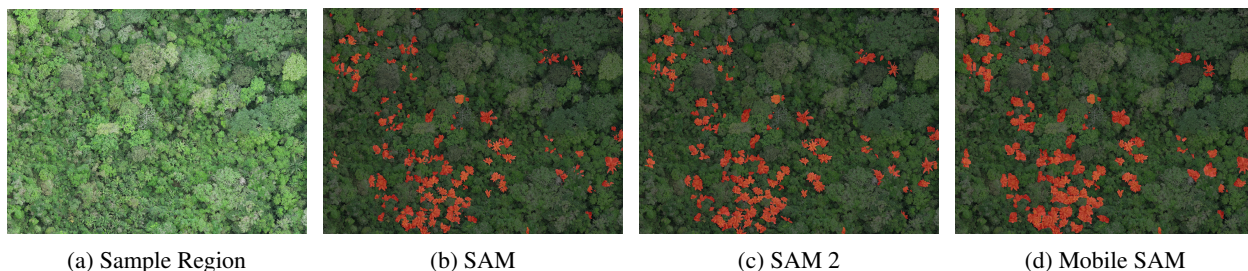


Figure 4: Segmentations of SAM and Mobile SAM.

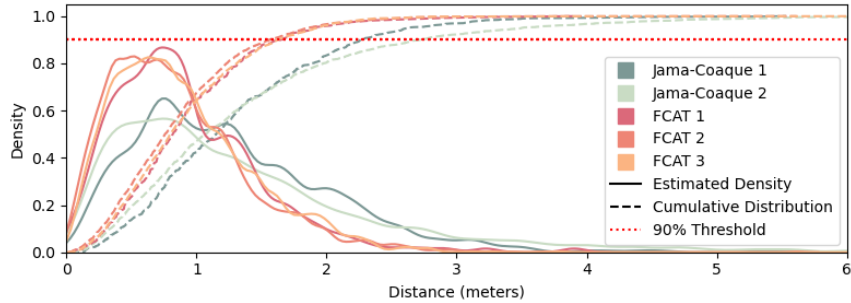
model size, all models maintain consistent inference times, processing at speeds exceeding 40 frames per second, thus ensuring their capability for real-time applications and suitability for on-board deployment.

Performance analysis reveals that more training data consistently enhances model performance in palm localization. With 90% of the data allocated for training, there is a noticeable improvement in Precision, Recall, and the quality of bounding boxes, as reflected in higher APs across thresholds. Notably, with only 10% of the data for training, YOLOv9 leads in detection performance, achieving an mAP of 0.59 and an AP_{75} of 0.64 – both over 6% higher than the nearest competitor. Its precision and recall also exceed the next best by more than 1%. Conversely, when trained with 90% of the data, RT-DETR excels, notably in mAP and AP_{75} , reaching 0.734 and 0.822, respectively, each about 5% higher than its closest competitor. These results suggest that ViT-based methods significant benefits from larger training sets, particularly in bounding box quality.

The visual comparison in Figure 3 using models trained with 90% data demonstrates their performance across varied scenarios. In the first row of Figure 3, YOLOv9 struggles with densely overlapped palm crowns, indicating difficulties in complex canopy textures, which is reflected in the saliency map focusing on non-palm tree crowns and leading to missed detections. In the second row, RT-DETR, while showing a slightly higher confidence in palm detection, produces two false positives in the bottom right corner due to a low confidence threshold set to improve recall. Its saliency map confirms a heightened focus in this area. Conversely, YOLOv8 exhibits a similar issue with a false alert on the top right, and YOLOv10, despite its precision, fails to accurately bound a palm leaf there. In the third row, all models perform robustly in a more straightforward setting, correctly identifying palms and proving their efficacy. The saliency maps reveal prioritization of palm leaves and centers, with centers often highlighted more intensely; however, they also display activities in non-palm zones, illustrating that while saliency maps guide model focus, the final detection head – comprising additional layers responsible for final decision-making – ultimately confirms the presence of palms, which shows the disparity between model attention and actual detection.

4.2.2 Segmentation

The segmentation outcomes from SAM, SAM 2, and Mobile SAM, compared in Figure 4, reflect their robust out-of-sample predictive performance in Jama-Coaque 1, a site in another reserve that is significantly different in rainfall, palm species, and forest structure from the environment of training samples. This demonstrates the adaptability of the detection model, despite some expected false alerts due to the set low confidence level in palm detection. SAM excels in boundary precision that closely matches the actual contours of palm leaves, though it may fragment palm crowns into multiple segments where they overlap with other tree crowns. SAM 2, however, outperforms



Statistics	FCAT 1	FCAT 2	FCAT 3	Jama-Coaque 1	Jama-Coaque 2
Mean (m)	0.90	0.84	0.84	1.20	1.30
Median (m)	0.77	0.73	0.74	1.06	1.05
Standard Deviation (m)	0.60	0.54	0.51	0.78	1.02

Figure 5: Distribution of Distance Shifts Across Sites.

Table 4: Latency of Different Configurations for PalmDSNet Across 5 Sites. Segmentation latency is measured based on the detection results of RT-DETR.

Model	FCAT 1	FCAT 2	FCAT 3	Jama-Coaque 1	Jama-Coaque 2
RT-DETR	42.9	378.0	273.5	177.1	143.0
YOLOv8	34.1	297.6	213.1	138.9	112.0
YOLOv9	34.7	297.2	216.4	140.4	113.8
YOLOv10	31.3	273.8	197.5	134.3	102.3
SAM	175.9	1454.9	1219.5	496.6	590.4
SAM 2	150.4	1265.4	1052.8	445.7	509.1
Mobile SAM	107.2	835.8	654.0	341.7	334.2

its predecessor by delivering better boundary segmentation while reducing the occurrence of small, broken segments that appears in SAM. At the same time, SAM 2 maintains a high level of segmentation performance, providing a more cohesive representation of palm crowns. In contrast, Mobile SAM includes broader areas as foreground, resulting in more unified palm segmentation but with less precise boundaries. All models perform commendably without supervision and demonstrate robust inference capabilities.

4.2.3 Counting

Table 3 evaluates the counting accuracy of detection models across five sites, assessing the impact of training data quantity. Counting accuracy is determined by the proximity of detected centers to labeled centers, with success defined as a center detected within a 5-meter radius of the labeled center. FCAT 1 and FCAT 2, marked with *, were used for training image patches and exhibit excellent performance at these sites and strong generalizability at FCAT 3, demonstrating robust model adaptability within the same ecological reserve. However, performance varies at different reserves, with RT-DETR consistently excelling at Jama-Coaque sites. Notably, the minimal variance between training with 10% and 90% of the data suggests that more extensive training improves object localization precision rather than overall detection efficiency.

Additionally, Figure 5 quantifies the palm localization performance across five sites by utilizing estimated density and cumulative distributions of distance shifts. These shifts often occur when bounding box centers do not align with actual palm centers, typically when only part of a palm is visible, causing the bounding box center to skew towards visible leaves. FCAT sites have significantly high performance, with mean distances under 0.90 meter and medians under 0.77 meters. In contrast, Jama-Coaque sites, which were not included in the training set, show slightly larger

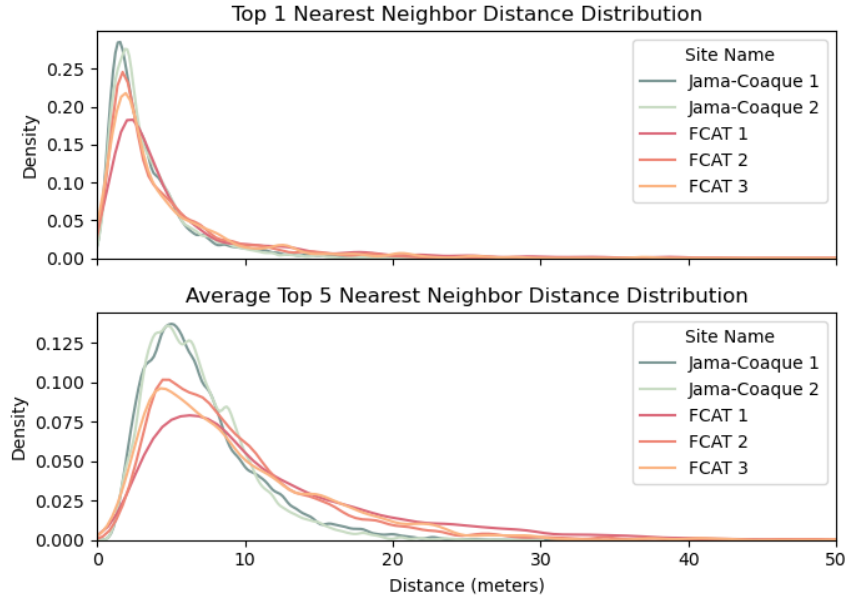


Figure 6: Distribution of Distances to Nearest Neighbors Among Detected Palm Centers Across Sites.

distance shifts, with means under 1.30 meters and medians less than 1.06 meters, yet still within the acceptable range under 5 meters.

Furthermore, FCAT sites display lower variability in distance shifts, with standard deviations ranging from 0.51 to 0.60 meters, compared to 0.78 to 1.02 meters for Jama-Coaque. This indicates more consistent palm localization in FCAT regions, possibly due to more homogeneous environmental conditions or better palm visibility in the dataset. The slightly larger variance observed in Jama-Coaque reflects the model’s greater difficulty in adapting to variability in forest composition and palm species. Nonetheless, the model demonstrates robust adaptability across diverse environments.

4.2.4 Real-time Processing

The latency data presented in Table 4 for PalmDSNet across five sites substantiates the framework’s capability for real-time processing, which is essential for immediate ecological assessments. In this context, detection (first 4 rows) refers to the process of identifying palms and saving all relevant information into a CSV file, while segmentation (last 3 rows) involves generating and saving the combined segmentation mask overlaid on the image. As demonstrated previously, our models maintain a high throughput, processing over 40 frames per second on an RTX 3090, which underscores their potential for real-time applications and suitability for on-board UAV deployment. Detection times vary from 31.3 to 378 seconds depending on the area size processed, and segmentation times, guided by palm counts and RT-DETR results, range from 107.2 to 1454.9 seconds. Overall, the processing times for detection, segmentation, and counting span from about two and a half minutes to half an hour per site, confirming the framework’s practicality for real-time use in varied environments.

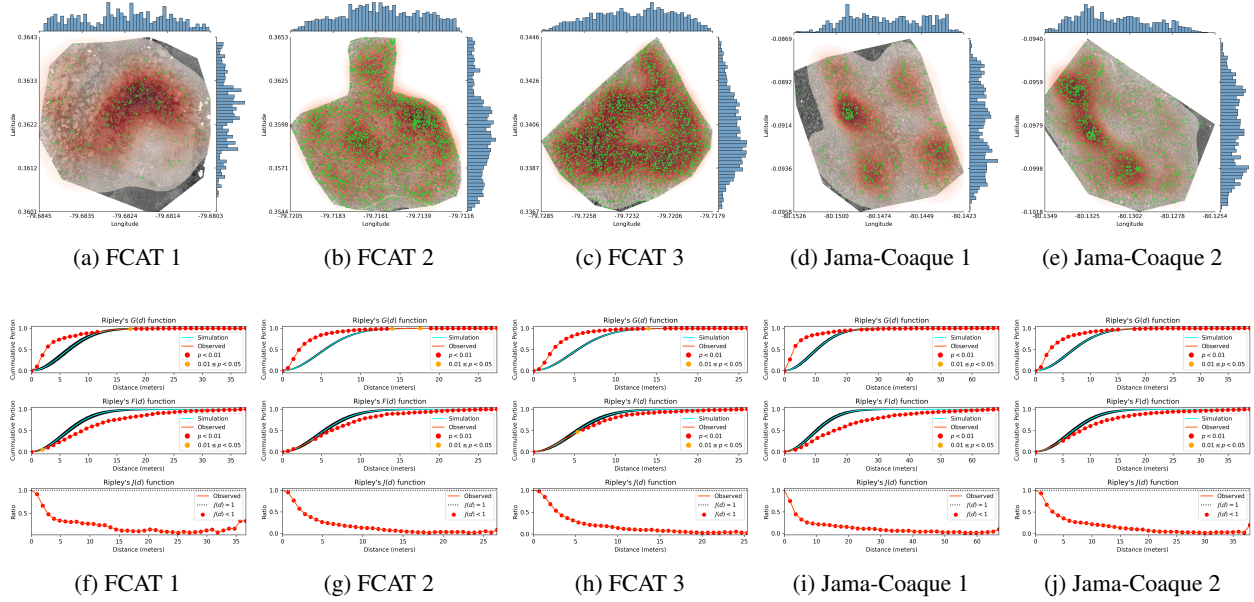


Figure 7: Visualization and Randomness Analysis of Palm Spatial Distribution. The first row (a-e) presents kernel density estimates with histograms illustrating palm distribution across regions. Green dots indicate detected palm locations, with darker KDE regions showing higher clustering. The second row (f-j) compares Ripley’s functions of the detected palms to those generated by a Poisson process, highlighting deviations from randomness. Blue-shaded areas represent the 95% confidence intervals with the black line indicating the mean for a Poisson process, while the red lines represent Ripley’s functions of the observed data. Red and orange points denote regions with p -values below 1% and 5%, respectively, indicating significant differences from randomness. These indices quantify palm clustering or dispersion relative to a random distribution.

Table 5: Parameters p^* and σ^* for different sites.

Parameters	FCAT 1	FCAT 2	FCAT 3	Jama-Coaque 1	Jama-Coaque 2
p^*	0.49	0.52	0.46	0.64	0.51
σ^*	50	70	70	80	60

4.3 Spatial Distribution Analysis

The analysis of spatial distribution in palm populations provides critical insights into their ecological dynamics and interspecies relationships. By examining spatial patterns, we can better understand species coexistence and competition, which are essential for guiding sustainable forest management and utilization strategies [50], [65]. This section explores various aspects of palm spatial distribution, including nearest neighbor analysis, distribution randomness, and simulation of spatial point patterns.

4.3.1 Analysis of Spatial Nearest Neighbors

Figure 6 depicts the distribution of distances from each detected palm to its nearest neighbors to explore their spatial arrangement. The distribution of nearest neighbor distance reveals a compact clustering of palms, indicating that palms often grow in close proximity, which suggests potential biological interactions or shared habitat preferences. The average top five nearest neighbors’ distance distribution shows that while palms generally form tight clusters, they also participate in larger, slightly more dispersed groups. Notably, this pattern is more distinct in Jama-Coaque than in FCAT, which reflects diverse ecological strategies and community structuring across different

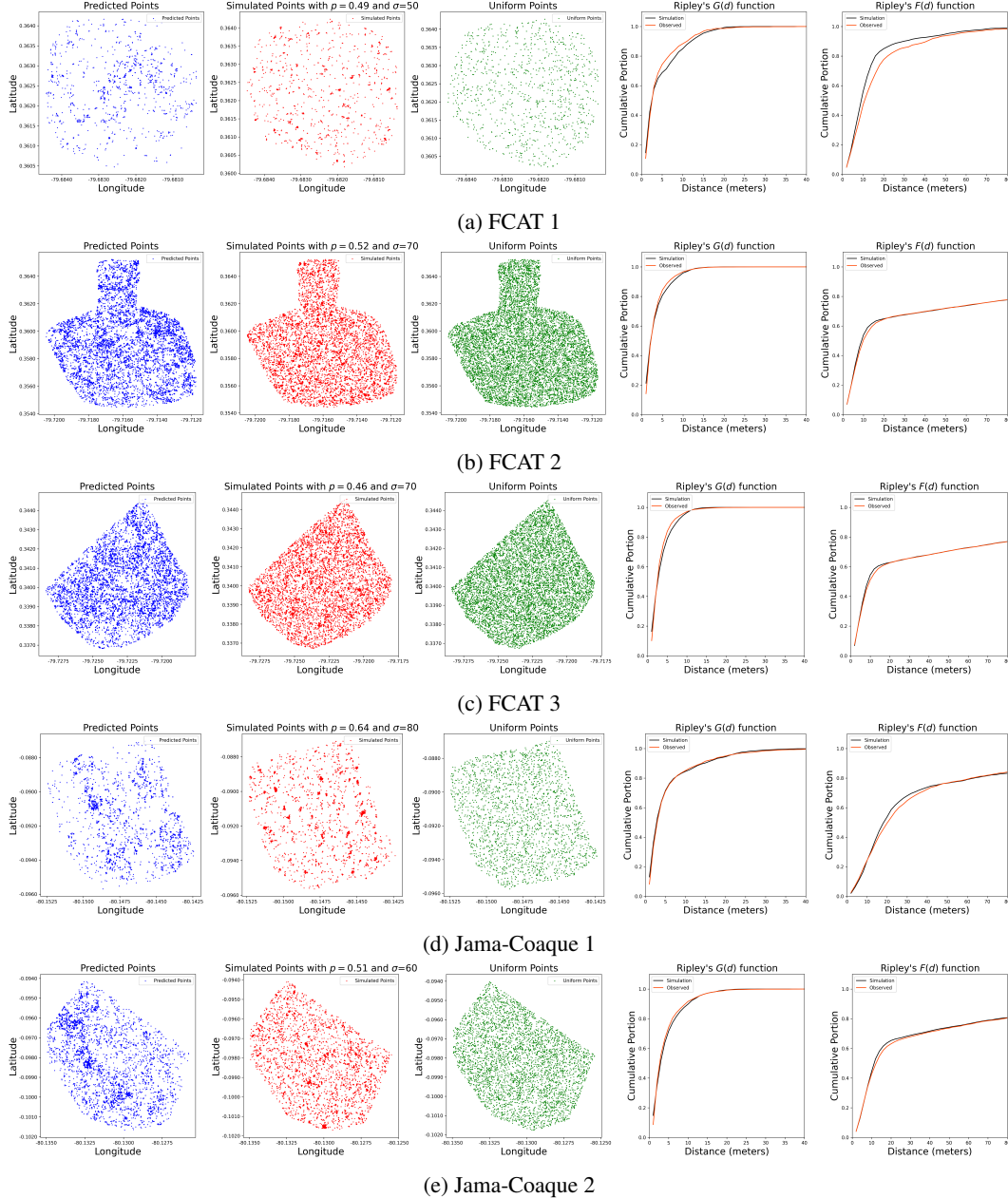


Figure 8: Comparison of Simulated and Predicted Point Patterns. The first column presents the predicted spatial distribution of detected palms by PalmDSNet, the second column shows the simulated distribution, and the third column depicts random points with a uniform distribution. The fourth and fifth columns compare Ripley’s G and F functions, respectively, between the simulated and predicted distributions.

reserves, with the contribution of endogenous demographic processes and environmental factors being a promising area for future research.

4.3.2 Analysis of Distribution Randomness

The primary objective of this analysis is to determine whether the spatial distribution of palms across various sites deviates from a random pattern. By comparing the observed palm distributions

with those generated by a Poisson point process, we aim to identify underlying ecological patterns that may indicate clustering or dispersion within these environments.

Figure 7 illustrates the spatial distribution of palms across the five study sites. These regions display varying levels of palm density, with certain areas exhibiting notably higher concentrations than others. The visualizations in the first row reveal that the palm distributions are not random; clusters and dispersed regions are clearly visible, suggesting non-random spatial arrangements. The second row of Figure 7 compares the observed point patterns of palm distributions with those generated by a Poisson point process using Ripley’s functions. For the G and F plots, the central black line represents the expected pattern if palms were randomly scattered throughout the forest. The blue-shaded area around this line indicates the 95% confidence interval within which random data points would typically fall, with different confidence levels ($1 - p$) for the sampled points being random, depicted with varying colors for $p < 0.01$ and $p < 0.05$. The J function plot includes a dashed line at $J(d) = 1$, with values below this line colored red to indicate clustering.

For the G function, the observed line ascends more steeply than the random case, indicating a higher degree of clustering among the palms, with palms closer to their nearest neighbors than they would be in a completely random distribution. Conversely, in the F function, the observed line falls below the random case, implying that random points must travel a greater distance to find a nearby palm, indicating larger gaps or empty spaces in the actual palm distribution compared to a random arrangement. The J function, with values below 1, further supports these observations by indicating that the palms are more clustered than would be expected under randomness. Together, these Ripley’s functions reveal significant deviations from randomness and suggest complex ecological interactions shaping palm distributions. The observed pattern’s clustering is more prominent than randomness yet less extreme than one would expect with a Student’s t distribution. This sets the stage for future work to explore the underlying ecological drivers of the distribution.

4.3.3 Simulation of Spatial Point Pattern

Given the statistically significant evidence that the distribution of palms is far from random, as anticipated due to the influence of various factors such as habitat suitability, as well as human and animal activities, we seek to employ a statistical yet straightforward model that can simulate and explain the spatial point patterns of palm distribution. To this end, we utilize the proposed Poisson-Gaussian palm reproduction model, which integrates the inherent stochastic nature of palm reproduction with spatially dependent factors, thereby generating distributions that can be compared with those predicted by PalmDSNet.

To measure clustering and dispersion in the simulated palm distributions, we use Ripley’s G and F functions, which quantify spatial patterns, with G indicating clustering and F showing dispersion. By comparing these functions from our simulations to those predicted by PalmDSNet, we aim to align the simulated distributions with the predicted ones. Ecologically, the parameter p indicates the likelihood of global randomness in palm distribution, with higher values denoting greater randomness and lower values indicating local clustering with a Gaussian distribution. The parameter σ represents the local range of palm reproduction, reflecting the degree of clustering around individual palms.

Table 5 lists the grid search results of the p^* and σ^* pairs for the five regions. Across the five sites, σ^* consistently ranges from 50 to 80 ($\sim 2-4$ m), and p^* values for four of the sites range from 0.46 to 0.52, both of which are quite stable. Jama-Coaque 1 is an exception, with a value of p^* of 0.64, indicating more dispersed clusters, as also reflected by the slightly larger σ^* for

this site. This greater dispersion is evident in the estimated density shown in Figure 7d. The robustness of p^* and σ^* across different forests demonstrates the model’s capability to capture the common point patterns of palm distributions, even with only two parameters. This simplicity helps in understanding the spread of palm species in forests under various scenarios.

Figure 8 compares our simulated point patterns to those predicted across five sites. The first column presents the predicted spatial distribution of detected palms by PalmDSNet, the second column shows the simulated distribution, and the third column depicts random points with a uniform distribution. The fourth and fifth columns compare Ripley’s G and F functions, respectively, between the simulated and predicted distributions. This last comparison shows an excellent fit for all sites. With the exception of FCAT 1, the simulated point patterns in the second column are visually more homogeneous than the predicted ones. This is easily explained by the fact that the distribution parameters were estimated globally. This observation should lead us to perform slightly more localized parameter estimation in the future.

5 Conclusion

In summary, our work with the PalmDSNet framework has proven to be effective in detecting, segmenting, and counting palms across diverse forest environments. We found that increasing the number of labels enhances the precision of bounding boxes, though it has a minimal impact on counting accuracy. The framework is also capable of real-time processing, even under resource-constrained conditions, including on-board UAV processing and integration into autonomous flight control systems. Additionally, our examination of palm distribution across two different forest reserves reveals that palms often form tightly-knit clusters, yet their spatial arrangements can differ significantly between forest ecosystems. The Poisson-Gaussian reproduction model, which employs a brute-force method to identify the best-fitting parameters that align with observed point patterns using Ripley’s G and F functions, has also shown satisfying performance. This model reliably captures the spatial patterns of palm distribution across various forest reserves, with consistent parameter values observed in most sites. By quantifying the level of clustering and its deviation from randomness, the Poisson-Gaussian reproduction model enhances our understanding of spatial processes of palms, which is crucial for environmental monitoring, conservation efforts, management strategies, economic planning, and supply chain optimization. Together, these two models provide an end-to-end solution, from image analysis to addressing ecological challenges.

In future work, we intend to expand our dataset through a semi-manual approach, wherein our trained model will assist in the labeling process. This expansion will include the annotation of additional sites in Ecuador, where data collection is feasible, enabling us to conduct species-level mapping to explore how spatial patterns evolve from the wettest forests in the Chocó to the limit of the tropical dry forest at the Sechura Desert, as well as a 1000 km² area in Amazonian forest near Iquitos, Peru. Besides using orthomosaics, we want to compare whether multiple views from raw UAV images, without processing, provide deeper insights into the canopy and improve detection of partially occluded palms, potentially revealing more hidden individuals. The established framework can also be readily adapted to address other conservation challenges [4], such as species-level identification of canopy trees, as well as the detection and segmentation of agriculture and forestry, and water bodies – the latter a task of significant importance for monitoring illegal mining activities and other environmental concerns [66], [67]. Furthermore, we will consider integrating more complex statistical models to refine the alignment of spatial patterns, including quantifying the importance of endogenous demographic processes as well as environmental predictors, and histor-

ical and current human effects on palm populations, particularly after incorporating species-level classifications.

References

- [1] W. L. Eiserhardt, J.-C. Svenning, W. D. Kissling, and H. Balslev, “Geographical ecology of the palms (arecaceae): Determinants of diversity and distributions across spatial scales,” *Annals of Botany*, vol. 108, no. 8, pp. 1391–1416, 2011.
- [2] N. Y. P. Zambrana, A. Byg, J.-C. Svenning, M. Moraes, C. Grandez, and H. Balslev, “Diversity of palm uses in the western amazon,” *Biodiversity and Conservation*, vol. 16, pp. 2771–2787, 2007.
- [3] W. J. Sutherland, R. P. Freckleton, H. C. J. Godfray, S. R. Beissinger, T. Benton, D. D. Cameron, *et al.*, “Identification of 100 fundamental ecological questions,” *Journal of ecology*, vol. 101, no. 1, pp. 58–67, 2013.
- [4] S. Camalan, K. Cui, V. P. Pauca, *et al.*, “Change detection of amazonian alluvial gold mining using deep learning and sentinel-2 imagery,” *Remote Sensing*, vol. 14, no. 7, p. 1746, 2022.
- [5] F. H. Wagner, R. Dalagnol, X. Tagle Casapia, *et al.*, “Regional mapping and spatial distribution analysis of canopy palms in an amazon forest using deep learning and vhr images,” *Remote Sensing*, vol. 12, no. 14, p. 2225, 2020.
- [6] N. C. Pitman, J. E. G. Andino, M. Aulestia, C. E. Cerón, D. A. Neill, W. Palacios, *et al.*, “Distribution and abundance of tree species in swamp forests of amazonian ecuador,” *Ecography*, vol. 37, no. 9, pp. 902–915, 2014.
- [7] Y. Malhi, T. A. Gardner, G. R. Goldsmith, M. R. Silman, and P. Zelazowski, “Tropical forests in the anthropocene,” *Annual Review of Environment and Resources*, vol. 39, pp. 125–159, 2014.
- [8] Y. van der Hoek, S. Álvarez Solas, and M. C. Peñuela, “The palm mauritia flexuosa, a keystone plant resource on multiple fronts,” *Biodiversity and Conservation*, vol. 28, no. 3, pp. 539–551, 2019.
- [9] J. Terborgh, “Community aspects of frugivory in tropical forests,” in *Frugivores and seed dispersal*, Springer, 1986, pp. 371–384.
- [10] K. Cui, Z. Shao, G. Larsen, V. Pauca, S. Alqahtani, D. Segurado, *et al.*, “Palmprobnet: A probabilistic approach to understanding palm distributions in ecuadorian tropical forest via transfer learning,” in *Proceedings of the 2024 ACM Southeast Conference*, 2024, pp. 272–277.
- [11] X. Tagle Casapia, L. Falen, H. Bartholomeus, *et al.*, “Identifying and quantifying the abundance of economically important palms in tropical moist forest using uav imagery,” *Remote Sensing*, vol. 12, no. 1, p. 9, 2019.
- [12] W. Li, H. Fu, L. Yu, and A. Cracknell, “Deep learning based oil palm tree detection and counting for high-resolution remote sensing images,” *Remote Sensing*, vol. 9, no. 1, p. 22, 2016.
- [13] M. Freudenberg, N. Nölke, A. Agostini, K. Urban, F. Wörgötter, and C. Kleinn, “Large scale palm tree detection in high resolution satellite images using u-net,” *Remote Sensing*, vol. 11, no. 3, p. 312, 2019.

- [14] J. Y. Park, H. C. Muller-Landau, J. W. Lichstein, S. W. Rifai, J. P. Dandois, and S. A. Bohlman, “Quantifying leaf phenology of individual trees and species in a tropical forest using unmanned aerial vehicle (uav) images,” *Remote Sensing*, vol. 11, no. 13, p. 1534, 2019.
- [15] M. B. A. Gibril, H. Z. M. Shafri, A. Shanableh, R. Al-Ruzouq, A. Wayayok, and S. J. Hashim, “Deep convolutional neural network for large-scale date palm tree mapping from uav-based images,” *Remote Sensing*, vol. 13, no. 14, p. 2787, 2021.
- [16] K. Cui and R. J. Plemmons, “Unsupervised classification of aviris-ng hyperspectral images,” in *2021 11th Workshop on Hyperspectral Imaging and Signal Processing: Evolution in Remote Sensing (WHISPERS)*, IEEE, 2021, pp. 1–5.
- [17] R. Muscarella, T. Emilio, O. L. Phillips, S. L. Lewis, F. Slik, W. J. Baker, *et al.*, “The global abundance of tree palms,” *Global Ecology and Biogeography*, vol. 29, no. 9, pp. 1495–1514, 2020.
- [18] C. G. Hidalgo Pizango, E. N. Honorio Coronado, J. del Águila-Pasquel, G. Flores Llampazo, J. de Jong, *et al.*, “Sustainable palm fruit harvesting as a pathway to conserve amazon peatland forests,” *Nature Sustainability*, vol. 5, no. 6, pp. 479–487, 2022.
- [19] K. Cui, R. Li, S. L. Polk, *et al.*, “Superpixel-based and spatially-regularized diffusion learning for unsupervised hyperspectral image clustering,” *IEEE Transactions on Geoscience and Remote Sensing*, 2024.
- [20] J. Zhang, S. Xu, Y. Zhao, J. Sun, S. Xu, and X. Zhang, “Aerial orthoimage generation for uav remote sensing,” *Information Fusion*, vol. 89, pp. 91–120, 2023.
- [21] Z. Qin, W. Wang, K.-H. Dammer, L. Guo, and Z. Cao, “Ag-yolo: A real-time low-cost detector for precise spraying with case study of palms,” *Frontiers in Plant Science*, vol. 12, p. 753 603, 2021.
- [22] T. Jintasuttisak, E. Edirisinghe, and A. Elbattay, “Deep neural network based date palm tree detection in drone imagery,” *Computers and Electronics in Agriculture*, vol. 192, p. 106 560, 2022.
- [23] M. Di Marco, S. Ferrier, T. D. Harwood, A. J. Hoskins, and J. E. Watson, “Wilderness areas halve the extinction risk of terrestrial biodiversity,” *Nature*, vol. 573, no. 7775, pp. 582–585, 2019.
- [24] Z. Zou, K. Chen, Z. Shi, Y. Guo, and J. Ye, “Object detection in 20 years: A survey,” *Proceedings of the IEEE*, vol. 111, no. 3, pp. 257–276, 2023.
- [25] N. Carion, F. Massa, G. Synnaeve, N. Usunier, A. Kirillov, and S. Zagoruyko, “End-to-end object detection with transformers,” in *European conference on computer vision*, Springer, 2020, pp. 213–229.
- [26] Y. Zhao, W. Lv, S. Xu, J. Wei, G. Wang, Q. Dang, *et al.*, *Detrs beat yolos on real-time object detection*, arXiv preprint arXiv:2304.08069, 2023. arXiv: 2304.08069.
- [27] G. Jocher, A. Chaurasia, and J. Qiu, *Ultralytics yolov8*, <https://github.com/ultralytics/ultralytics>, version 8.0.0, Accessed: 2024-05-10, 2023.
- [28] C.-Y. Wang, I.-H. Yeh, and H.-Y. M. Liao, *Yolov9: Learning what you want to learn using programmable gradient information*, arXiv preprint arXiv:2402.13616, 2024. arXiv: 2402.13616 [cs.CV].
- [29] A. Wang, H. Chen, L. Liu, *et al.*, *Yolov10: Real-time end-to-end object detection*, arXiv preprint arXiv:2405.14458, 2024. arXiv: 2405.14458 [cs.CV].

- [30] T. Diwan, G. Anirudh, and J. V. Tembhurne, “Object detection using yolo: Challenges, architectural successors, datasets and applications,” *multimedia Tools and Applications*, vol. 82, no. 6, pp. 9243–9275, 2023.
- [31] C.-Y. Wang, H.-Y. M. Liao, Y.-H. Wu, P.-Y. Chen, J.-W. Hsieh, and I.-H. Yeh, “Cspnet: A new backbone that can enhance learning capability of cnn,” in *Proceedings of the IEEE/CVF conference on computer vision and pattern recognition workshops*, 2020, pp. 390–391.
- [32] A. Kirillov, E. Mintun, N. Ravi, H. Mao, C. Rolland, L. Gustafson, *et al.*, “Segment anything,” in *Proceedings of the IEEE/CVF International Conference on Computer Vision*, 2023, pp. 4015–4026.
- [33] N. Ravi, V. Gabeur, Y.-T. Hu, *et al.*, “Sam 2: Segment anything in images and videos,” *arXiv preprint arXiv:2408.00714*, 2024.
- [34] C. Zhang, D. Han, Y. Qiao, *et al.*, *Faster segment anything: Towards lightweight sam for mobile applications*, arXiv preprint arXiv:2306.14289, 2023. arXiv: 2306.14289.
- [35] C. Zhang, L. Liu, Y. Cui, *et al.*, *A comprehensive survey on segment anything model for vision and beyond*, arXiv preprint arXiv:2305.08196, 2023. arXiv: 2305.08196.
- [36] A. Dosovitskiy, L. Beyer, A. Kolesnikov, D. Weissenborn, X. Zhai, T. Unterthiner, *et al.*, “An image is worth 16x16 words: Transformers for image recognition at scale,” *arXiv preprint arXiv:2010.11929*, 2020.
- [37] K. He, X. Chen, S. Xie, Y. Li, P. Dollár, and R. Girshick, “Masked autoencoders are scalable vision learners,” in *Proceedings of the IEEE/CVF conference on computer vision and pattern recognition*, 2022, pp. 16 000–16 009.
- [38] C. Ryali, Y.-T. Hu, D. Bolya, *et al.*, “Hiera: A hierarchical vision transformer without the bells-and-whistles,” in *International Conference on Machine Learning*, PMLR, 2023, pp. 29 441–29 454.
- [39] G. Hinton, O. Vinyals, and J. Dean, “Distilling the knowledge in a neural network,” *arXiv preprint arXiv:1503.02531*, 2015.
- [40] I. Petritan, R. Marzano, A. M. Petritan, and E. Lingua, “Overstory succession in a mixed quercus petraea–fagus sylvatica old growth forest revealed through the spatial pattern of competition and mortality,” *Forest Ecology and Management*, vol. 326, pp. 9–17, 2014.
- [41] K. Gadow, C. Zhang, C. Wehenkel, *et al.*, “Forest structure and diversity,” *Continuous Cover Forestry, Book Series Managing Forest Ecosystems*, vol. 23, pp. 29–83, 2012.
- [42] F. May, A. Huth, and T. Wiegand, “Moving beyond abundance distributions: Neutral theory and spatial patterns in a tropical forest,” *Proceedings. Biological sciences / The Royal Society*, vol. 282, 2015.
- [43] G. Jia, X. Yu, D. Fan, and J. Jia, “Mechanism underlying the spatial pattern formation of dominant tree species in a natural secondary forest,” *PLoS ONE*, vol. 11, 2016.
- [44] B. D. Ripley, *Spatial statistics*. Wiley, 1981.
- [45] A. Baddeley, E. Rubak, and R. Turner, *Spatial point patterns: Methodology and applications with R*. CRC Press, Taylor & Francis Group, 2016.
- [46] C. X. Garzón López, P. Jansen, S. Bohlman, A. Ordonez, and H. Olff, “Effects of sampling scale on patterns of habitat association in tropical trees,” *Journal of Vegetation Science*, vol. 25, May 2013.
- [47] P. Haase, “Spatial pattern analysis in ecology based on ripley’s k-function: Introduction and methods of edge correction,” *Journal of Vegetation Science*, vol. 6, pp. 575–582, 1995.

- [48] J. Besag, “Contribution to the discussion on dr. ripley’s paper,” *Journal of the Royal Statistical Society: Series B (Methodological)*, vol. 39, no. 2, pp. 193–195, 1977.
- [49] F. Goreaud, “Apports de l’analyse de la structure spatiale en forêt tempérée à l’étude et la modélisation des peuplements complexes,” *Dissertation*, 2000.
- [50] M. Ben-Said, “Spatial point-pattern analysis as a powerful tool in identifying pattern-process relationships in plant ecology: An updated review,” *Ecological Processes*, vol. 10, pp. 1–23, 2021.
- [51] E. Velázquez, I. Martínez Cano, S. Getzin, K. Moloney, and T. Wiegand, “An evaluation of the state of spatial point pattern analysis in ecology,” *Ecography*, vol. 39, 2016.
- [52] T. Wiegand and K. A. Moloney, “Rings, circles, and null-models for point pattern analysis in ecology,” *Oikos*, vol. 104, pp. 209–229, 2004.
- [53] I. Renner, J. Elith, A. Baddeley, *et al.*, “Point process models for presence-only analysis,” *Methods in Ecology and Evolution*, vol. 6, 2015.
- [54] M. Carrer, D. Castagneri, P. Ionel, M. Pividori, and E. Lingua, “Tree spatial patterns and stand attributes in temperate forests: The importance of plot size, sampling design, and null model,” *Forest Ecology and Management*, vol. 417, pp. 125–134, 2018.
- [55] R. Law, J. Illian, D. Burslem, G. Gratzer, C. Gunatilleke, and N. Gunatilleke, “Ecological information from spatial patterns of plants: Insights from point process theory,” *Journal of Ecology*, vol. 97, pp. 616–628, 2009.
- [56] M. Jácome-Flores, M. Delibes, T. Wiegand, and J. Fedriani, “Spatial patterns of an endemic mediterranean palm recolonizing old fields,” *Ecology and Evolution*, vol. 6, pp. 1–13, Nov. 2016. DOI: 10.1002/ece3.2504.
- [57] L. Browne and J. Karubian, “Diversity of palm communities at different spatial scales in a recently fragmented tropical landscape,” *Botanical Journal of the Linnean Society*, vol. 182, no. 2, pp. 451–464, 2016.
- [58] S. Lueder, K. Narasimhan, J. Olivo, *et al.*, “Functional traits, species diversity, and species composition of a neotropical palm community vary in relation to forest age,” *Frontiers in Ecology and Evolution*, vol. 10, p. 678 125, 2022.
- [59] R. R. Selvaraju, M. Cogswell, A. Das, R. Vedantam, D. Parikh, and D. Batra, “Grad-cam: Visual explanations from deep networks via gradient-based localization,” in *Proceedings of the IEEE international conference on computer vision*, 2017, pp. 618–626.
- [60] J. Gildenblat and contributors, *Pytorch library for cam methods*, <https://github.com/jacobgil/pytorch-grad-cam>, 2021.
- [61] J. F. C. Kingman, *Poisson processes*. Clarendon Press, 1992, vol. 3.
- [62] J. S. Clark, M. Silman, R. Kern, E. Macklin, and J. HilleRisLambers, “Seed dispersal near and far: Patterns across temperate and tropical forests,” *Ecology*, vol. 80, no. 5, pp. 1475–1494, 1999.
- [63] M. R. Metz, W. P. Sousa, and R. Valencia, “Widespread density-dependent seedling mortality promotes species coexistence in a highly diverse amazonian rain forest,” *Ecology*, vol. 91, no. 12, pp. 3675–3685, 2010.
- [64] F. B. Hildebrand, *Introduction to numerical analysis*. Courier Corporation, 1987.
- [65] S. Tao, N. Labrière, K. Calders, *et al.*, “Mapping tropical forest trees across large areas with lightweight cost-effective terrestrial laser scanning,” *Annals of Forest Science*, vol. 78, no. 4, p. 103, 2021.

- [66] K. Cui, S. Camalan, R. Li, *et al.*, “Semi-supervised change detection of small water bodies using rgb and multispectral images in peruvian rainforests,” in *2022 12th Workshop on Hyperspectral Imaging and Signal Processing: Evolution in Remote Sensing (WHISPERS)*, IEEE, 2022, pp. 1–5.
- [67] S. Camalan, K. Cui, P. Pauca, *et al.*, “Detecting change due to alluvial gold mining in peruvian rainforest using recursive convolutional neural networks and contrastive learning,” in *AGU Fall Meeting Abstracts*, vol. 2022, 2022, B52G–0905.